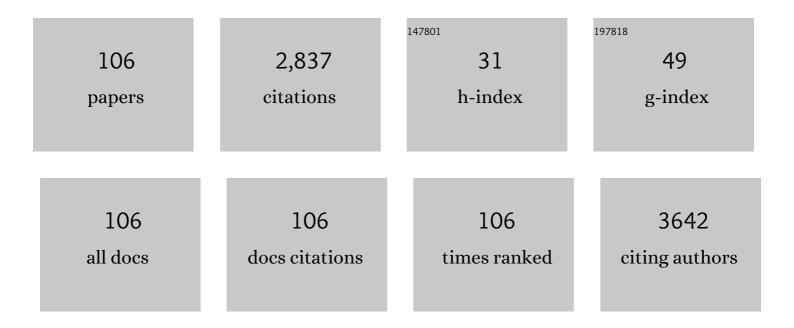


List of Publications by Year in descending order

Source: https://exaly.com/author-pdf/2722639/publications.pdf Version: 2024-02-01



Bolu

#	Article	IF	CITATIONS
1	Ultrasensitive acetone gas sensor can distinguish the diabetic state of people and its high performance analysis by first-principles calculation. Sensors and Actuators B: Chemical, 2022, 351, 130863.	7.8	39
2	Fabrication of a high-efficiency CdS@TiO ₂ @C/Ti ₃ C ₂ composite photocatalyst for the degradation of TC-HCl under visible light. New Journal of Chemistry, 2022, 46, 3305-3314.	2.8	7
3	Silver nanoparticles decorated reduced graphene oxide: Eco-friendly synthesis, characterization, biological activities and embryo toxicity studies. Environmental Research, 2022, 210, 112864.	7.5	17
4	Hierarchical Ag3PO4/TiO2@C composites derived from Ti3C2 MXene for enhanced photocatalytic activity. Journal of Materials Science, 2022, 57, 5396-5409.	3.7	4
5	Study on the Arsenate Removal from Raw As(V)-Rich Wastewater Using Zero-Valent Iron. Water (Switzerland), 2022, 14, 1118.	2.7	3
6	Hollow MoS ₂ Spheres Confined in Carbon Fibers for Ultralong-life Potassium Storage. ACS Applied Energy Materials, 2022, 5, 3605-3614.	5.1	9
7	Highly sensitive and stable H2 gas sensor based on p-PdO-n-WO3-heterostructure-homogeneously-dispersing thin film. International Journal of Hydrogen Energy, 2022, 47, 17821-17834.	7.1	21
8	Tumor microenvironment responsive nanogels as a smart triggered release platform for enhanced intracellular delivery of doxorubicin. Journal of Biomaterials Science, Polymer Edition, 2021, 32, 385-404.	3.5	10
9	A strategy to prepare activated carbon fiber membranes for flexible solid-state supercapacitor applications. Journal of Materials Science, 2021, 56, 3911-3924.	3.7	13
10	Enhanced photocatalytic performance of electrospun hollow titanium dioxide nanofibers decorated with graphene quantum dots. Journal of Materials Science, 2021, 56, 2138-2149.	3.7	10
11	An overview on the incorporation of graphene quantum dots on TiO2 for enhanced performances. Journal of Materials Science, 2021, 56, 6031-6051.	3.7	14
12	Carbon-coated WS ₂ nanosheets supported on carbon nanofibers for high-rate potassium-ion capacitors. Energy and Environmental Science, 2021, 14, 3184-3193.	30.8	100
13	Janus 2D titanium nitride halide TiNX _{0.5} Y _{0.5} (X, Y = F, Cl, or Br, and X ≠Y) monolayers with giant out-of-plane piezoelectricity and high carrier mobility. Physical Chemistry Chemical Physics, 2021, 23, 3637-3645.	2.8	15
14	In-situ fabrication of ZnO nanoparticles sensors based on gas-sensing electrode for ppb-level H ₂ S detection at room temperature*. Chinese Physics B, 2021, 30, 020701.	1.4	11
15	Super response and selectivity to H2S at room temperature based on CuO nanomaterials prepared by seed-induced hydrothermal growth. Materials and Design, 2021, 201, 109507.	7.0	24
16	Fabrication of in-situ grown and Pt-decorated ZnO nanoclusters on new-type FTO electrode for room-temperature detection of low-concentration H2S. Journal of Alloys and Compounds, 2021, 860, 158499.	5.5	22
17	Adsorption of Sb(III) from Aqueous Solution by nZVI/AC: A Magnetic Fixed-Bed Column Study. Nanomaterials, 2021, 11, 1912.	4.1	2
18	Improvement of Gas Sensing of Uniform Ag ₃ PO ₄ Nanoparticles to NH ₃ under the Assistant of LED Lamp with Low Power Consumption at Room Temperature. ChemistrySelect, 2021, 6, 8338-8344.	1.5	4

#	Article	IF	CITATIONS
19	Electrospun Nanofibers of Polycaprolactone/Collagen as a Sustained-Release Drug Delivery System for Artemisinin. Pharmaceutics, 2021, 13, 1228.	4.5	40
20	Electrospun Nanofibers of Natural and Synthetic Polymers as Artificial Extracellular Matrix for Tissue Engineering. Nanomaterials, 2021, 11, 21.	4.1	115
21	Removal of Antimony(V) from Drinking Water Using nZVI/AC: Optimization of Batch and Fix Bed Conditions. Toxics, 2021, 9, 266.	3.7	2
22	Identify the Nematic Superconductivity of Topological Superconductor Pd\$\$_x\$\$Bi\$\$_2\$\$Te\$\$_3\$\$ by Angle-dependent Upper Critical Field Measurement. Journal of Superconductivity and Novel Magnetism, 2021, 34, 3045-3052.	1.8	3
23	Investigate the Nb doping position and its relationship with bulk topological superconductivity in NbxBi2Se3 by X-ray photoelectron spectra. Journal of Physics and Chemistry of Solids, 2020, 137, 109208.	4.0	9
24	Precise generation of dynamic biochemical signals by controlling the programmable pump in a Yâ€shaped microfluidic chip with a "christmas tree―inlet. Electrophoresis, 2020, 41, 883-890.	2.4	10
25	Deformation behavior and texture evolution in an extruded Mg Li sheet with non-basal texture during tensile deformation. Materials Characterization, 2020, 159, 110041.	4.4	16
26	The 2D Porous g-C ₃ N ₄ /CdS Heterostructural Nanocomposites with Enhanced Visible-Light-Driven Photocatalytic Activity. Journal of Nanoscience and Nanotechnology, 2020, 20, 1098-1108.	0.9	9
27	Highly sensitive H2 sensor based on PdO-decorated WO3 nanospindle p-n heterostructure. International Journal of Hydrogen Energy, 2020, 45, 31327-31340.	7.1	41
28	Removal of Molybdenum(VI) from Raw Water Using Nano Zero-Valent Iron Supported on Activated Carbon. Water (Switzerland), 2020, 12, 3162.	2.7	8
29	Low-temperature operating ZnO-based NO ₂ sensors: a review. RSC Advances, 2020, 10, 39786-39807.	3.6	82
30	Synthesis and room-temperature H2S sensing of Pt nanoparticle-functionalized SnO2 mesoporous nanoflowers. Journal of Alloys and Compounds, 2020, 842, 155813.	5.5	31
31	Preparation of a g-C3N4/UiO-66-NH2/CdS Photocatalyst with Enhanced Visible Light Photocatalytic Activity for Tetracycline Degradation. Nanomaterials, 2020, 10, 1824.	4.1	19
32	Adsorption Kinetics of Arsenic (V) on Nanoscale Zero-Valent Iron Supported by Activated Carbon. Nanomaterials, 2020, 10, 1791.	4.1	16
33	A microfluidic platform enabling real-time control of dynamic biochemical stimuli to biological cells. Journal of Micromechanics and Microengineering, 2020, 30, 095011.	2.6	5
34	Enhanced H2S gas sensing properties by the optimization of p-CuO/n-ZnO composite nanofibers. Journal of Materials Science, 2020, 55, 7702-7714.	3.7	39
35	Fabrication of ZnO Nanoparticles Modified by Uniformly Dispersed Ag Nanoparticles: Enhancement of Gas Sensing Performance. ACS Omega, 2020, 5, 5209-5218.	3.5	75
36	Real-Time Analysis of the Stability of Oil-In-Water Pickering Emulsion by Electrochemical Impedance Spectroscopy. Molecules, 2020, 25, 2904.	3.8	2

#	Article	IF	CITATIONS
37	Porous Graphitic Carbon Fibers for Fastâ€Charging Supercapacitor Applications. Energy Technology, 2020, 8, 2000050.	3.8	14
38	In Situ Growing Double-Layer TiO ₂ Nanorod Arrays on New-Type FTO Electrodes for Low-Concentration NH ₃ Detection at Room Temperature. ACS Applied Materials & Interfaces, 2020, 12, 8573-8582.	8.0	52
39	Formulation Strategies for Folate-Targeted Liposomes and Their Biomedical Applications. Pharmaceutics, 2019, 11, 381.	4.5	71
40	Fabrication of 2D Hetero-Complexes With Nucleic-Acid-Base Adenine and Fatty-Acid Stearic Acid at Liquid/Solid Interface. Frontiers in Chemistry, 2019, 7, 513.	3.6	0
41	A Comprehensive Outlook of Synthetic Strategies and Applications of Redoxâ€Responsive Nanogels in Drug Delivery. Macromolecular Bioscience, 2019, 19, e1900071.	4.1	42
42	The fabrication of gold colloidal nanoantennas by a full wet surface assembly technique. Applied Physics Express, 2019, 12, 064008.	2.4	7
43	Preparation of Lutein-Loaded PVA/Sodium Alginate Nanofibers and Investigation of Its Release Behavior. Pharmaceutics, 2019, 11, 449.	4.5	46
44	Selective Dye Adsorption by Zeolitic Imidazolate Framework-8 Loaded UiO-66-NH2. Nanomaterials, 2019, 9, 1283.	4.1	49
45	Synthesis of ZnO Hierarchical Structures and Their Gas Sensing Properties. Nanomaterials, 2019, 9, 1277.	4.1	36
46	Enhanced cobalt-based catalysts through alloying ruthenium to cobalt lattice matrix as an efficient catalyst for overall water splitting. Electrochimica Acta, 2019, 327, 134958.	5.2	24
47	Flexibility and thermal dynamic stability increase of dsDNA induced by Ru(bpy)2dppz2+ based on AFM and HRM technique. BMC Chemistry, 2019, 13, 68.	3.8	1
48	Controlled Growth of LDH Films with Enhanced Photocatalytic Activity in a Mixed Wastewater Treatment. Nanomaterials, 2019, 9, 807.	4.1	22
49	Antibacterial Properties of Graphene-Based Nanomaterials. Nanomaterials, 2019, 9, 737.	4.1	301
50	Low-Cost and High-Performance ZnO Nanoclusters Gas Sensor Based on New-Type FTO Electrode for the Low-Concentration H2S Gas Detection. Nanomaterials, 2019, 9, 435.	4.1	34
51	Fabrication of CdS quantum dots sensitized ZnO nanorods/TiO2 nanosheets hierarchical heterostructure films for enhanced photoelectrochemical performance. Electrochimica Acta, 2019, 304, 334-341.	5.2	51
52	Recent Developments in the Interactions of Classic Intercalated Ruthenium Compounds: [Ru(bpy)2dppz]2+ and [Ru(phen)2dppz]2+ with a DNA Molecule. Molecules, 2019, 24, 769.	3.8	14
53	Simultaneous cross-linking and pore-forming electrospun carbon nanofibers towards high capacitive performance. Applied Surface Science, 2019, 479, 128-136.	6.1	50
54	Blotting Paper-Derived Activated Porous Carbon/Reduced Graphene Oxide Composite Electrodes for Supercapacitor Applications. Molecules, 2019, 24, 4625.	3.8	12

#	Article	IF	CITATIONS
55	Enhanced photodegradation activity of electrospun porous TiO2 fibers. Functional Materials Letters, 2019, 12, 1941002.	1.2	6
56	Solar Concentrator Consisting of Multiple Aspheric Reflectors. Energies, 2019, 12, 4038.	3.1	0
57	Hierarchical Fe2O3 nanorods/TiO2 nanosheets heterostructure: Growth mechanism, enhanced visible-light photocatalytic and photoelectrochemical performances. Applied Surface Science, 2019, 475, 380-388.	6.1	34
58	Suppression of resonant auger effect with chirped x-ray free-electron laser pulse. Journal of Physics B: Atomic, Molecular and Optical Physics, 2018, 51, 035602.	1.5	2
59	Controllable Fabrication of Au-Coated AFM Probes via a Wet-Chemistry Procedure. Nanoscale Research Letters, 2018, 13, 366.	5.7	9
60	The Mechanism of Adsorption, Diffusion, and Photocatalytic Reaction of Organic Molecules on TiO2 Revealed by Means of On-Site Scanning Tunneling Microscopy Observations. Catalysts, 2018, 8, 616.	3.5	5
61	Effect of Surfactants on the Microstructures of Hierarchical SnO2 Blooming Nanoflowers and their Gas-Sensing Properties. Nanoscale Research Letters, 2018, 13, 250.	5.7	22
62	Facile preparation of nitrogen-enriched hierarchical porous carbon nanofibers by Mg(OAc)2-assisted electrospinning for flexible supercapacitors. Applied Surface Science, 2018, 456, 827-834.	6.1	29
63	A Roadmap for Achieving Sustainable Energy Conversion and Storage: Graphene-Based Composites Used Both as an Electrocatalyst for Oxygen Reduction Reactions and an Electrode Material for a Supercapacitor. Energies, 2018, 11, 167.	3.1	20
64	An Effective Utilization of Solar Energy: Enhanced Photodegradation Efficiency of TiO2/Graphene-Based Composite. Energies, 2018, 11, 630.	3.1	3
65	Tactile-Sensing Based on Flexible PVDF Nanofibers via Electrospinning: A Review. Sensors, 2018, 18, 330.	3.8	158
66	Preferred conformational structures of disaccharides with β-1,4-linked N-acetylglucosamine and D-mannose in the gas phase: A tree-step computational approach study. Computational and Theoretical Chemistry, 2018, 1140, 24-31.	2.5	2
67	Atomic Force Microscopy Based Tip-Enhanced Raman Spectroscopy in Biology. International Journal of Molecular Sciences, 2018, 19, 1193.	4.1	24
68	Characterization of Inter- and Intramolecular Interactions of Amyloid Fibrils by AFM-Based Single-Molecule Force Spectroscopy. Journal of Nanomaterials, 2016, 2016, 1-18.	2.7	8
69	Investigating the Co-Adsorption Behavior of Nucleic-Acid Base (Thymine and Cytosine) and Melamine at Liquid/Solid Interface. Nanoscale Research Letters, 2016, 11, 552.	5.7	5
70	Self-assembly of hydrogen-bonded supramolecular complexes of nucleic-acid-base and fatty-acid at the liquid–solid interface. Physical Chemistry Chemical Physics, 2016, 18, 14168-14171.	2.8	18
71	Investigation of the non-covalent interactions of molecular self-assembly by scanning tunneling microscopy using the association of aromatic structures in pyrene-4,5,9,10-tetraone and phenanthrene-9,10-dione molecules. RSC Advances, 2015, 5, 103316-103320.	3.6	7
72	An insight into hydration structure of sodium glycinate from ab initio quantum chemical study. Journal of Molecular Modeling, 2015, 21, 234.	1.8	4

#	Article	IF	CITATIONS
73	A tree-step computational approach to simplify conformational determination of cellobiose and lactose. Carbohydrate Research, 2015, 401, 51-57.	2.3	3
74	Predicting the structural preferences of luteolin-7-O-β-d-glucoside in the gas phase: An application of the hybrid MCMM/QM approach. Computational and Theoretical Chemistry, 2015, 1051, 42-46.	2.5	0
75	Exploring the complex mechanical properties of xanthan scaffolds by AFM-based force spectroscopy. Beilstein Journal of Nanotechnology, 2014, 5, 365-373.	2.8	6
76	A Comparison of Theoretical and Experimental Raman Spectra of Microhydrated Sodium Glycinate. Advanced Materials Research, 2014, 934, 116-120.	0.3	0
77	Nanomechanics of phospholipid LB film studied layer by layer with AFM. Chemistry Central Journal, 2014, 8, 71.	2.6	4
78	Ab initio investigation of the first hydration shell of protonated glycine. Journal of Chemical Physics, 2014, 140, 085103.	3.0	12
79	Light-driven fluorescence enhancement and self-assembled structural evolution of an azobenzene derivative. Journal of Materials Chemistry C, 2014, 2, 9866-9873.	5.5	24
80	Migration of defect clusters and xenon-vacancy clusters in uranium dioxide. International Journal of Modern Physics B, 2014, 28, 1450120.	2.0	2
81	Morphology and Wettability Tunable Organogel System Based on An 1,3,4-Oxadiazole Derivative. Soft Materials, 2014, 12, 396-402.	1.7	9
82	Predicting the preferred conformations of luteolin-4′-O-β-D-glucoside in gas phase: a comparison of two computational approaches. Journal of Molecular Modeling, 2013, 19, 3619-3626.	1.8	5
83	Determining the structural preferences of dimannosides through the linkage constraint and hydrogen-bonded network. Computational and Theoretical Chemistry, 2013, 1010, 45-52.	2.5	8
84	Surface-enhanced Raman spectroscopy investigation on human breast cancer cells. Chemistry Central Journal, 2013, 7, 37.	2.6	46
85	Migration of point defects and a defect pair in zinc oxide using the dimer method. Journal of Materials Research, 2012, 27, 2241-2248.	2.6	7
86	Direct force producing uniform ultra-thin chitosan films by atomic force microscopy. RSC Advances, 2012, 2, 2732.	3.6	6
87	Collagen coated tantalum substrate for cell proliferation. Colloids and Surfaces B: Biointerfaces, 2012, 95, 10-15.	5.0	17
88	Building layer-by-layer 3D supramolecular nanostructures at the terephthalic acid/stearic acid interface. Chemical Communications, 2011, 47, 9155.	4.1	13
89	Building the First Hydration Shell of Deprotonated Glycine by the MCMM and ab Initio Methods. Journal of Physical Chemistry B, 2011, 115, 6213-6221.	2.6	14
90	Oriented growth of single NaCl (100) crystal induced by Langmuir–Blodgett film. Journal of Materials Research, 2011, 26, 230-235.	2.6	2

#	Article	IF	CITATIONS
91	Hydration of Sugars in the Gas Phase: Regioselectivity and Conformational Choice in <i>N</i> â€Acetyl Glucosamine and Glucose. Chemistry - A European Journal, 2009, 15, 13427-13434.	3.3	38
92	Electronâ€Captureâ€Induced Dissociation of Microsolvated Di―and Tripeptide Monocations: Elucidation of Fragmentation Channels from Measurements of Negative Ions. ChemPhysChem, 2009, 10, 1619-1623.	2.1	9
93	Conformational flexibility of phycocyanobilin: Monte-Carlo and DFT study. Computational and Theoretical Chemistry, 2009, 894, 9-13.	1.5	11
94	Two-dimensional scaffold layer formations on a solid surface through xanthan polysaccharide: Temperature effect. Colloids and Surfaces B: Biointerfaces, 2009, 74, 136-139.	5.0	6
95	Influence of Tunable External Stimuli on the Self-Assembly of Guanosine Supramolecular Nanostructures Studied By Atomic Force Microscope. Langmuir, 2009, 25, 13432-13437.	3.5	14
96	Electron-capture—Induced dissociation of protoporphyrin IX ions. Journal of the American Society for Mass Spectrometry, 2008, 19, 809-813.	2.8	11
97	Anti-Influenza Virus Activities of Flavonoids from the Medicinal PlantElsholtzia rugulosa. Planta Medica, 2008, 74, 847-851.	1.3	101
98	Carbohydrate molecular recognition: a spectroscopic investigation of carbohydrate–aromatic interactions. Physical Chemistry Chemical Physics, 2007, 9, 4444.	2.8	71
99	On the Mechanism of Electron-Capture-Induced Dissociation of Peptide Dications from15N-Labeling and Crown-Ether Complexation. Journal of Physical Chemistry A, 2007, 111, 9641-9643.	2.5	48
100	IR-Spectral Signatures of Aromatic–Sugar Complexes: Probing Carbohydrate–Protein Interactions. Angewandte Chemie - International Edition, 2007, 46, 3644-3648.	13.8	92
101	Electron capture induced dissociation of peptide ions: Identification of neutral fragments from secondary collisions with cesium vapor. International Journal of Mass Spectrometry, 2007, 263, 66-70.	1.5	37
102	Spectral signatures and structural motifs in isolated and hydrated monosaccharides: phenyl α- and β-l-fucopyranoside. Physical Chemistry Chemical Physics, 2006, 8, 129-136.	2.8	43
103	Building Up Key Segments ofN-Glycans in the Gas Phase: Intrinsic Structural Preferences of the α(1,3) and α(1,6) Dimannosides. Journal of the American Chemical Society, 2006, 128, 1976-1981.	13.7	38
104	Hydrogen loss from nucleobase nitrogens upon electron attachment to isolated DNA and RNA nucleotide anions. Journal of Chemical Physics, 2004, 121, 4175-4179.	3.0	19
105	Electron capture induced dissociation of peptide dications. International Journal of Mass Spectrometry, 2003, 225, 83-87.	1.5	62
106	Coulomb Explosion upon Electron Attachment to a Four-Coordinate Monoanionic Metal Complex. Journal of the American Chemical Society, 2003, 125, 9592-9593.	13.7	30